JOURNAL OF MATERIALS SCIENCE 33 (1998) 913–921

Constrained densification in boehmite–alumina mixtures for the fabrication of porous alumina ceramics

S. KWON, G. L. MESSING
Department of Materials Science and Engineering and The Particulate Materials Centre, Pennsylvania State University, University Park, PA 16802 USA

It is demonstrated that inherent constrained densification characteristics of the bimodal size distributed powders can be utilized to fabricate porous alpha alumina. Seeded boehmite was mixed with coarse alpha alumina particles to produce various compositions of bimodal mixtures. The densification behaviour of the mixtures was correlated with shrinkage and microstructural evolution. The mixtures sintered at 1200 °C contained more than 30% porosity and the mechanical strength of the mixtures was increased by 2–4 fold relative to the coarse particles alone with similar porosity (< 5 MPa). © *1998 Chapman & Hall*

1. Introduction

Porous ceramics have a wide range of applications including filters, desiccants, insulators, catalyst carriers, bone replacement, acoustic absorbers, and heat exchangers [1–3]. They are used in environments which require corrosion and abrasion resistance, and thermal stability. Ceramic filters can be fabricated by extrusion, injection of a ceramic slurry into a plastic foam body, chemical leaching, and sintering [1, 4]. The sintering method utilizes conventional densification and the pore size is controlled by adjusting the initial particle size or sintering temperature.

Porous materials generally have a poor mechanical strength because strength is inversely related to porosity. The mechanical strength, which can limit the application of porous ceramics, can be improved by using reinforcements or capsule-free hot isostatic pressing [3–6]. The sintering of sintered porous ceramics requires a temperature range where densification is low, porosity is retained, and considerable neck growth between particles can be achieved. The thermal stability of pores largely depends on the sintering temperature. Slow densification kinetics at high temperature is thus favourable to develop thermally stable pores and a reasonable mechanical strength.

One little explored approach to produce porous materials is to take advantage of the retarded densification phenomenon of powders with a bimodal particle size distribution. The densification of such powders is significantly retarded for several reasons. First, crack-like defects can evolve which relax the stress that arises in the matrix surrounding the non-densifying coarse particles [7, 8]. Secondly, differential densification between the matrix and the coarse particles, causes a compressive radial stress and a tensile hoop stress in the matrix. The tensile stress counteracts the sintering pressure of the matrix and inhibits densification of the mixture [9–11]. Bordia and Scherer [12] and Scherer [13] have pointed out that the tensile stresses or "backstress" cannot be greater than the sintering stress which is significantly less than previously reported. Lange has addressed the effect of the inclusion (i.e., coarse particle) spacing on the densification of a mixture by assuming the inclusions formed a dispersed network and the network shrinks in an undistorted manner [14]. Based on this idea, Sudre and Lange provided microstructural evidence for the development of a compressive stress in the matrix for inclusions more closely spaced than the average separation distance. In contrast tensile stresses arise in the matrix between the inclusions that are spaced further apart than the average separation distance in α-Al_2O_3 matrix and ZrO_2 mixtures [15]. Upon densification, the matrix under compressive stress densifies faster and becomes rigid. When the necks between inclusions interconnect to form a continuous network, further densification of the sample is significantly limited.

In the present work, a bimodal mixture of seeded boehmite and uniformly sized coarse α-Al_2O_3 particles was used to fabricate porous α-Al_2O_3 ceramics. By using α-Al_2O_3 seeded boehmite it will be shown that a higher strength can be achieved than solely with the α-Al_2O_3 and also that the porosity can be maximized as a result of the specific volume difference between boehmite and α-Al_2O_3. The retarded densification of the mixture was analysed by correlating the shrinkage and microstructural evolutions. The porosity, pore size distribution, and mechanical strength as well as their densification behaviour were investigated as a function of composition and sintering temperature.

2. Experimental procedure

A hydrosol was prepared by dispersing 15 wt % of commercial boehmite powder (Catapal D, Condea, Houston TX) in distilled water and adjusting the dispersion pH to 3 with nitric acid. The stabilized boehmite hydrosol was mixed with 1.5 wt % α-Al_2O_3 seeds obtained by the centrifugal method [16]. The coarse α-Al_2O_3 particle dispersion was prepared by mixing a commercial α-Al_2O_3 powder (AA2 Sumitomo Chemical America, Inc., New York, NY) in distilled water after adjusting the pH to 3 with nitric acid. The dispersions were stirred for 2 days and sonicated to break up agglomerates. The mean particle size of the coarse α-Al_2O_3 powder was 2 μm. Seeded boehmite sols were mixed with the coarse α-Al_2O_3 dispersions to produce 0, 30, 50, 70 and 100% α-Al_2O_3 mixtures. The compositions of the mixed sols are listed in Table I. Hereafter, the composition of mixtures will be referred to on the basis of the transformed state.

The mixed sol was gelled by dehydration on a hot plate and dried at 85 °C to produce gel fragments. The gel fragments of the mixtures were ground using an alumina mortar and pestle to <90 μm (-170 mesh) and redispersed in ethanol to obtain deformable agglomerates for pressing [16]. The dispersion was carried out by milling ground gel fragments for 10 h in a Nalgene™ plastic bottle using high purity alumina balls. Ethanol-dispersed mixtures were dried, ground, and sieved again to <90 μm. Sieved agglomerates were uniaxially pressed into pellets using a 12.7 mm diameter cylindrical steel die at 5 MPa and pellets were cold isostatically pressed at 280 MPa. The green density of the pellets was determined from the dimensions.

Pellets were heated in air from room temperature to 850 °C at a rate of 5 °C min^{-1} and from 850 °C to the sintering temperature at a rate of 15 °C min^{-1}. The samples were sintered at temperatures in the range of 1200–1600 °C for 100 min. The sintered densities were measured using the Archimedes technique. Microstructures of either polished or fractured surfaces of selected samples were observed by scanning electron microscopy (SEM). Polished samples were thermally etched at 50 °C below the sintering temperature for 30 min to reveal the grain structure. The mechanical strength of the sintered samples was determined by diametral compression at a constant crosshead speed of 0.5 mm min^{-1}. The sintered density was measured by the Archimedes technique and the pore size distribution was measured by mercury porosimetry. Continuous shrinkage of selected samples was measured with a thermomechanical analyser (TMA 60-5-5, Shimadzu).

3. Results

In a bimodal powder mixture, the composition of maximum packing, w_{f*}, can be calculated from:

$$w_{f*} = \frac{v_c - v_0}{v_f + v_c - v_0} \quad (1)$$

where v_c is the specific volume of the coarse particle compact (0.417 $cm^3\ g^{-1}$ in the present work), v_f is the specific volume of the fine particle compact (0.605 $cm^3\ g^{-1}$ in the present work), and v_0 is the theoretical specific volume of the α-Al_2O_3 (0.251 $cm^3\ g^{-1}$). The calculated w_{f*} value for the mixture is 0.218 $cm^3\ g^{-1}$ and the theoretically predicted density at w_{f*} is 80.6%. The theoretical packing volume of mixtures, v_{w_f} can be calculated from:

$$v_{w_f} = v_c(1 - w_f) \quad (\text{when } 0 \leqslant w_f \leqslant w_{f*}) \quad (2)$$

$$v_{w_f} = v_f + (1 - w_f)(v_0 - v_f) \quad (\text{when } w_{f*} \leqslant w_f \leqslant 1) \quad (3)$$

The theoretical and measured specific volumes of the mixtures are compared in Fig. 1. In region I, coarse particles are in contact and fine particles fill the voids between the coarse particles ($w_f \leqslant w_{f*}$), and in region II, coarse particles are dispersed in the fine particle matrix ($w_f \geqslant w_{f*}$). The compositions of the unfired mixtures are included in region II, and the theoretical packing density at $w_f = 0.36$ (referred to as the 70 mixture in Table I) is 74.0%. The difference between the theoretically predicted green density and the experimental data is due to mixing inhomogeneity [17, 18].

The green densities of the mixtures show typical bimodal mixture characteristics in Fig. 1; the $\sim$70% α-Al_2O_3 (coarse particle) sample has the maximum density and the density decreases as the boehmite (fine particle) content increases. The 100% α-Al_2O_3 sample is $\sim$60% dense, which indicates that the particles are randomly close packed.

Samples were heated for 5 min at 1200 °C to ensure complete transformation of boehmite to α-Al_2O_3. As seen in Fig. 2, the trend in the green density of the mixtures was not retained after transformation. The

TABLE I The seeded boehmite fraction and green densities of mixtures (fractions are based on solid phase only)

Name (based on α-Al_2O_3 fraction)	Weight fraction in green body (wt %)	Volume fraction in green body (vol %)	Theoretical density of green body (g/cm^3)	After α-Al_2O_3 transformation (%)
0 mixture	100	100	3.01	100
30 mixture	75.4	80.2	3.20	70
50 mixture	56.8	63.5	3.36	50
70 mixture	36.1	42.7	3.57	30
100 mixture	0	0	3.98	0

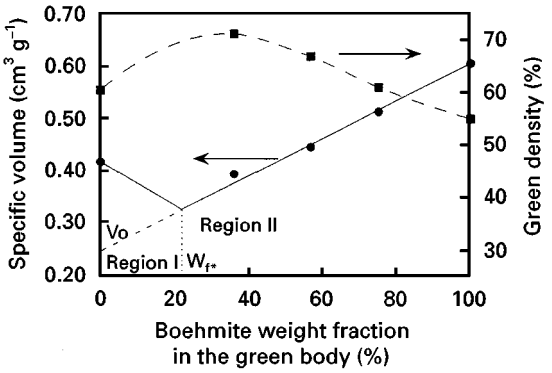

Figure 1 The green densities and specific volumes of the mixtures. Key: (●) specific volume and (—) ideal volume.

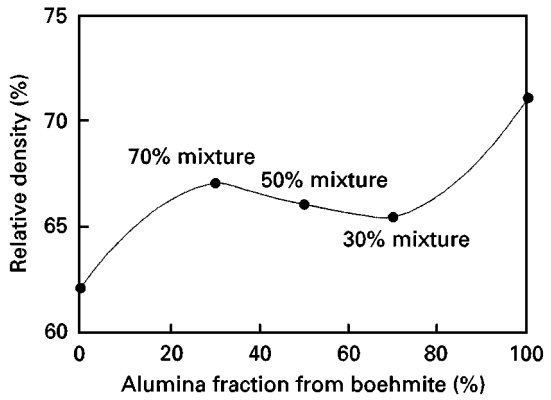

Figure 2 The density of the mixtures after α-Al_2O_3 transformation (heated at 1200 °C for 5 min).

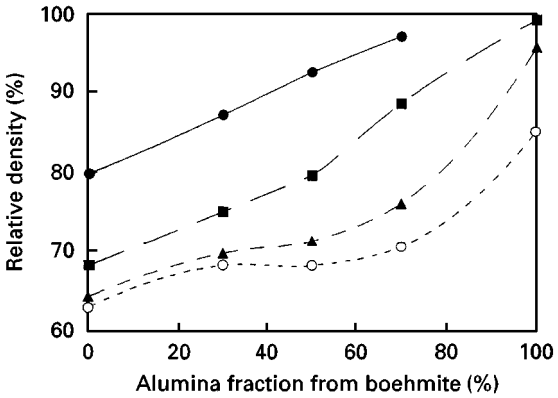

Figure 3 The density of the mixtures (after sintering for 100 min at sintering temperatures of: (○) 1200 °C, (▲) 1250 °C, (■) 1400 °C and (●) 1600 °C.

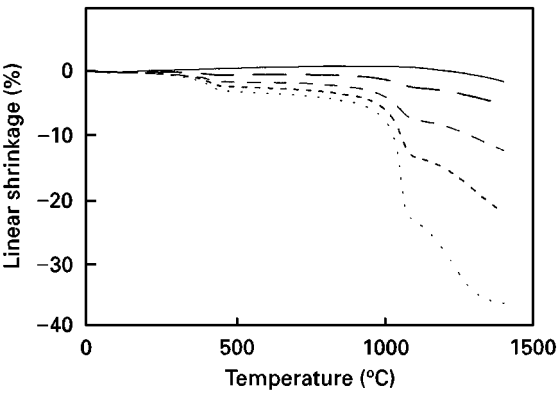

Figure 4 Measured linear shrinkage at a heating rate of 5 °C min^{-1} before 850 °C and 15 °C min^{-1} after 850 °C for the: (···) seeded boehmite, (- - -) 30% mixture, (– – –) 50% mixture, (——) 70% mixture and (——) coarse 100%.

67.1% density of the 70% mixture is lower than the green density (71.1%) because of the characteristics of the boehmite to α-Al_2O_3 phase transformation. The boehmite to γ-Al_2O_3 transformation, which is the first step of the sequential transformation of boehmite, is pseudomorphic and the weight loss due to dehydration is not accompanied by a change in external dimensions [19, 20]. Consequently, the transformed γ-Al_2O_3 has a sponge-like, porous texture [21] and the relative density of the sample during the transition alumina phase decreases relative to the initial boehmite sample. The transformation from boehmite to α-Al_2O_3 is accompanied by an $\sim$36% volume change. During this transformation, the presence of coarse α-Al_2O_3 particles can inhibit the shrinkage of the matrix in the same manner as in retarded densification. The densities at various temperatures are shown in Fig. 3 as a function of composition. It is clear that densification is significantly inhibited by the presence of the coarse α-Al_2O_3 particles, especially at 1200 and 1250 °C.

Fig. 4 shows the continuous shrinkage behaviour of mixtures and the two end members measured under the same heating profile as used in the sintering study. For the seeded boehmite, there is a large, abrupt shrinkage at $\sim$1100 °C which is due to the transformation of θ-Al_2O_3 to α-Al_2O_3. The shrinkage of the mixtures decreased as the coarse α-Al_2O_3 fraction increases. It should be noted that the coarse α-Al_2O_3 particle fractions in the 50 and 70% mixtures (0.24 and 0.41 respectively on the basis of the total sample volume) are much higher than the empirically determined threshold value for the formation of a three dimensional percolative network of inclusions, 0.16. When the inclusions form a percolative network, the shrinkage of the mixtures is the same as the shrinkage of the coarse particle compact. However, Fig. 4, shows that there is no evidence for the formation of a percolative network even in the 70% mixture.

Fig. 5 (a and b) shows the fracture surface of seeded boehmite and the 70% mixture after 5 min at 1200 °C. The transformed seeded boehmite in Fig. 5a has a crystallite size slightly smaller than 0.2 μm which is similar to previous reports for seeded boehmite [22–24]. The microstructure of the 70% mixture, in Fig. 5b, shows $\sim$1 μm scale voids formed between the coarse α-Al_2O_3 particles. These voids form because the seeded boehmite matrix recedes from the boehmite-α-Al_2O_3 particle interface during shrinkage. The transformed phase in the mixture is not as dense as the unconstrained seeded boehmite and the connectivity of the crystallites is also not as good as observed in the free sintered seeded boehmite.

Fig. 6 (a–f) compares the microstructure of the 30 and 70% mixtures sintered at 1200, 1250 and 1400 °C for 100 min. Fracture surfaces were examined for the samples sintered at 1200 °C and polished surfaces were

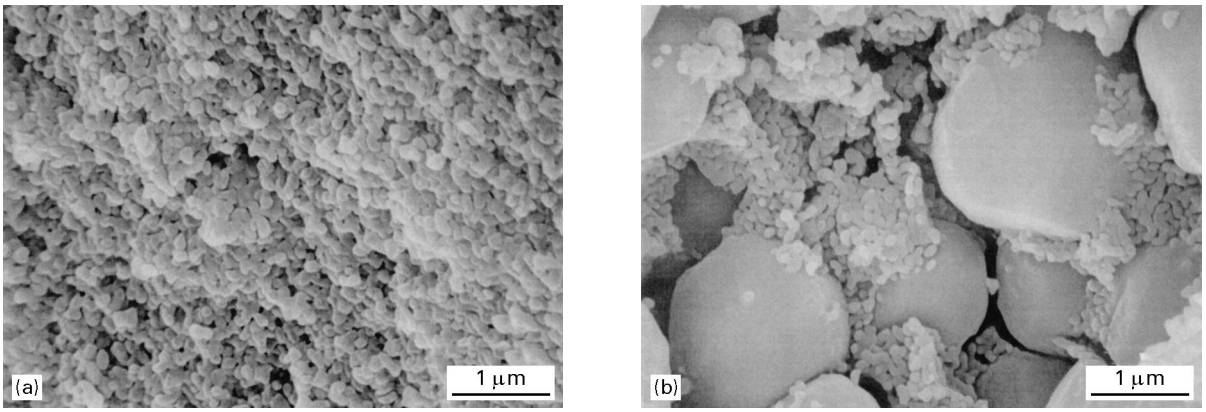

Figure 5 The fracture surface of transformed samples (a) seeded boehmite and (b) 70% mixture.

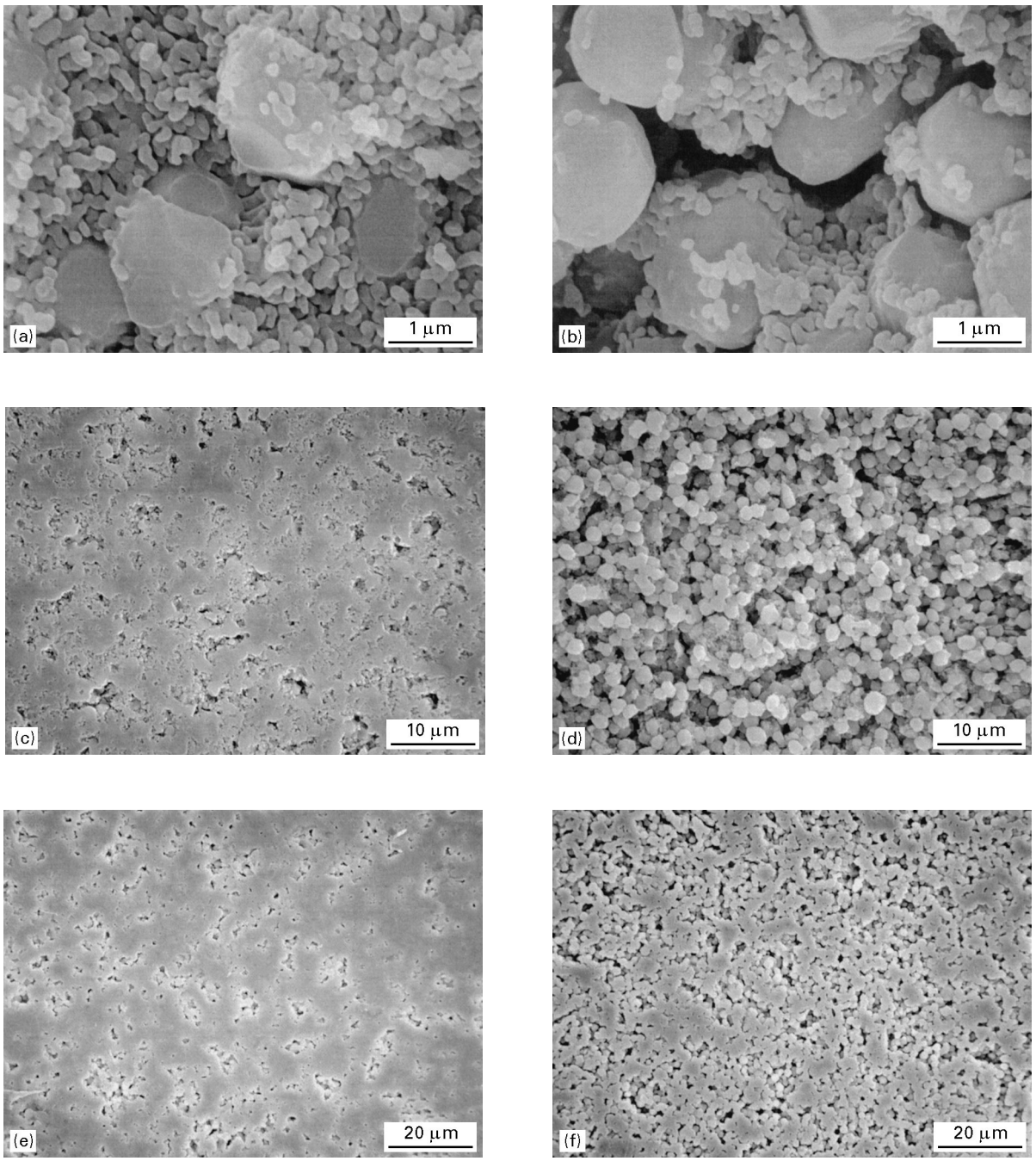

Figure 6 The microstructures of sintered samples (a) 30% mixture at 1200 °C, (b) 70% mixture at 1200 °C, (c) 30% mixture at 1250 °C, (d) 70% mixture at 1200 °C, (e) 30% mixture at 1400 °C and (f) 70% mixture at 1400 °C.

examined for the rest of the samples. At 1200 °C, the 30% mixture shows coarse α-Al_2O_3 particles dispersed in the fine matrix and the attachment of some fine particles to the coarse particles. In the 70% mixture, the coarse α-Al_2O_3 particles are very closely spaced or touching and large voids between coarse α-Al_2O_3 particle and matrix are observed. As the 30% mixture densifies, a dense matrix forms between the coarse particles at 1250 °C. Meanwhile, no significant densification is observed in the matrix of the 70% mixture at 1250 °C. At 1400 °C the dense area increases in the 30% mixture and the overall microstructure appears to form a continuous network. Fig. 6d still shows poor densification of the 70% mixture at 1400 °C and some neck formation between coarse particles and the early stage of continuous network development.

The pore size distributions of samples sintered at 1200 °C for 5 min are compared in Fig. 7. The two end members and the 30% alumina mixture have very narrow pore size distributions and it is broadened for the 50 and 70% mixtures. The most frequent pore size in the 100% coarse α-Al_2O_3 sample is 0.5 μm which is an order of magnitude larger than the pore size of the seeded boehmite (0.03 μm). The mixtures have pore size distributions between the coarse alumina and seeded boehmite end members and in accordance with the coarse α-Al_2O_3 content. The increased pore size of mixtures compared to that of the seeded boehmite is a reflection of retarded densification.

The strength of samples sintered at various conditions is shown in Fig. 8. The strength was calculated from:

$$\sigma = \frac{2P}{\pi D t} \tag{4}$$

where P is the load at fracture, D is the sample diameter (~ 10 mm), and t is the sample thickness. Samples were typically 3 mm thick and 10 mm in diameter. As expected from the low density and the lack of interparticle neck formation, the 100% alumina sample has very low strength regardless of the sintering condition. It is clear that the strength of the mixtures increases as the boehmite fraction increases and the trend is consistent with the sintered density.

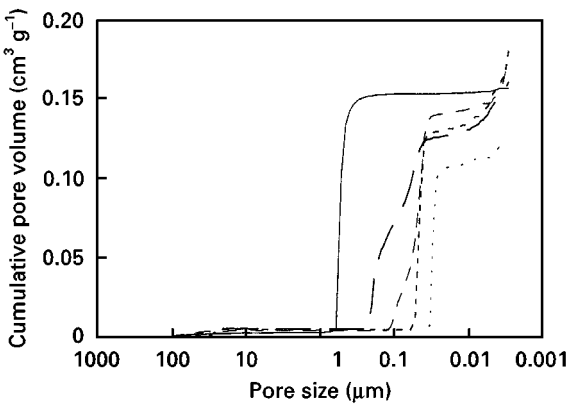

Figure 7 Cumulative pore size distributions of samples sintered at 1200 °C for 5 min. Key: (···) seeded boehmite, (- - -) 30% mixture, (– – –) 50% mixture, (——) 70% mixture and (——) 100% coarse.

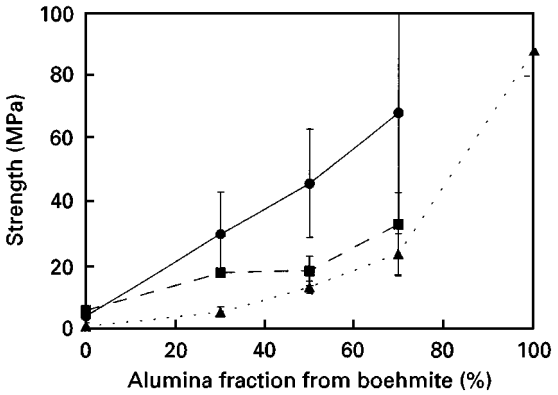

Figure 8 Diametral strength of samples sintered at (▲) 1200 °C for 5 min, (–) (■) 1250 °C for 100 min and (●) 1400 °C for 100 min.

4. Discussion

4.1. Density after α-Al_2O_3 transformation

It is useful to correlate the decreased relative density of the 70% mixture after the α-Al_2O_3 transformation with its composition and the specific volume change of the seeded boehmite. The volume fraction of coarse α-Al_2O_3 particles after transformation (volume of the inclusion particles divided by the total volume of the sample including pores), X_s^α, is related to the α-Al_2O_3 volume fraction in the green body, X_0^α, as:

$$X_s^\alpha = X_0^\alpha \frac{V_0}{V_s} \tag{5}$$

since the volume of α-Al_2O_3 particles does not change during heating, where V_s is the total sample volume after heating, and V_0 is the initial total volume. The sample volumes before and after heating are related as:

$$V_s/V_0 = (1-\varepsilon)^3 \tag{6}$$

where ε is the linear shrinkage.

In the green state, the solid phase of the 70% mixture consists of 42.7 vol% boehmite and 57.3 vol% α-Al_2O_3 (Table I). Based on the green density, the powder mixture consists of 30.4 vol% boehmite, 40.7 vol% α-Al_2O_3 (X_0^α), and 28.9 vol% porosity. The linear shrinkage of the 70% mixture, after heating at 1200 °C for 5 min, as measured by thermo mechanical analyser (TMA), was 4.5%. Using the above relationship, the X_s^α of this mixture can be calculated to be 46.7%. The volume fraction of the transformed phase X_s^b can be calculated as $X_s^\alpha 30/70$ because the mixture is designed to produce 30% of the α-Al_2O_3 from boehmite. The pore volume fraction of the transformed 70% mixture is $100 - X_s^\alpha - X_s^b$ or 33.3%. This value closely matches the measured porosity, which is 32.9%. The lower sample density after transformation results from a combination of the large specific volume change during transformation and the small shrinkage of the sample at 1200 °C.

4.2. Shrinkage and densification behaviour

If the green microstructure is assumed to be ideal, i.e., the α-Al_2O_3 particles are uniformly spaced in the seeded boehmite matrix, the separation distance

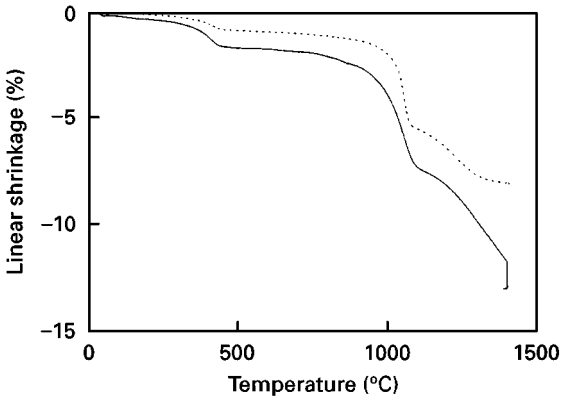

Figure 9 Measured and (···) calculated linear shrinkage of the 50% mixture.

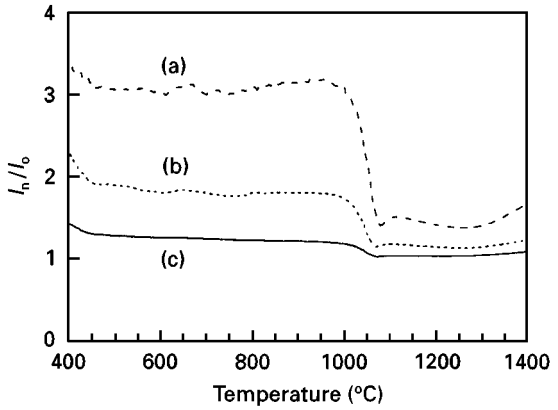

Figure 10 Calculated α value for (a) the 30% mixture, (b) the 50% mixture and (c) the 70% mixture.

between the neighbouring particles, d, and the particle radius, r, are related as:

$$2r/(2r + d) = (f/s)^{1/3} \quad (7)$$

where f is the volume fraction of the coarse particle and s is the coarse particle volume fraction at the maximum packing [14]. If the shrinkage of the mixture is purely from the matrix, the mixture shrinkage, ε_c, can be expressed as:

$$\varepsilon_c = \varepsilon_m[d/(2r + d)] \quad (8)$$

where ε_m is the matrix shrinkage. This expression assumes that shrinkage of the matrix between the closest coarse particles is the same as that of the free matrix.

Since the coarse particles do not contribute to the shrinkage, the matrix between particles spaced farther than d can not shrink as much as the matrix between the closest particles unless the particle network is deformed by shrinkage. If the matrix between the closest particle shrinks as much as in the unconstrained case, the total volume shrinkage of the entire matrix becomes much less than for unconstrained shrinkage. Fig. 9 illustrates that the predicted shrinkage of the 50% mixture is considerably less than the measured shrinkage if it is assumed that the matrix between the closest inclusions shrinks in a similar manner to the unconstrained case. It is clear that the matrix between the closest particles shrinks more than the unconstrained case to produce the measured shrinkage.

Lange [14] has introduced the numerical factor α, defined as l_n/l_0 where l_n is the particle separation distance (from centre to centre) where the matrix between the particles shrinks in a similar manner to the unconstrained case, and l_0 is the minimum particle separation distance $(2r + d)$. By incorporating α, the shrinkage of a mixture can be expressed as:

$$\varepsilon_c = \varepsilon_m[1 - (1/\alpha)(f/s)^{1/3}] \quad (9)$$

The theoretical shrinkage for a mixture can be estimated in the absence of extensive information, such as sintering stress and plastic deformation, using α. In the present work, shrinkage of the mixtures was measured and the α value for the mixtures was calculated by comparing the shrinkage with that of the free matrix (seeded boehmite). Fig. 10 shows the calculated α values for the mixtures. It is apparent that there is a discontinuity in the α values at the α-Al_2O_3 transformation temperature. As predicted by Lange, the α value is close to 1 when the inclusion fraction is high (70% mixture). The α values of the 50 and 30% mixtures are significantly greater than 1 even though a conservative value of 0.6 is chosen as the maximum particle volume fraction, f, based on the green density of the 100% alumina compact. The physical meaning of an α value >1 is that the matrix between the closest particles must be forced to shrink more than the free matrix, thus Lange chose 1 as the α value to interpret previous data reported by De Jonghe *et al.* [25].

The high α values in the present work are believed to be related to the matrix characteristics. Generally, shrinkage of a sample is accompanied by densification and the neck formation of the particles is accompanied by densification. However, in the present mixtures, the shrinkage before the α-Al_2O_3 transformation is from the specific volume change during phase transformation. Thus, it is believed that there is no significant neck formation between the particles in the matrix. The stresses developed in the matrix, produced by differential shrinkage, can be relieved by the particle rearrangement or grain boundary sliding [26]. Therefore, it is clear that, for the initial stage of shrinkage ($<1000\,^{\circ}C$) in the present work, the constraint is less severe than when actual densification is accompanied by neck formation between particles. In addition, it is apparent that for compositions experiencing a phase transformation, the shrinkage of the mixtures cannot be predicted solely by one α value for the entire range of densification.

The high α value observed even after transformation can also be due to the density difference between the unconstrained boehmite and constrained matrix phase in the mixtures as shown in Fig. 6 (a–f). If the crystallite packing of the transformed matrix phase is different from the free-transformed case, direct utilization of free matrix shrinkage to predict the shrinkage of mixtures is inappropriate. The density of the matrix,

ρ_m, can be calculated as follows:

$$\rho_m = \frac{X_s^b}{1 - X_s^\alpha} \quad (10)$$

The volume fraction of the transformed phase, X_s^b, is related to the relative sample density, ρ, by $X_s^b = \rho X_s^{b'}$, where $X_s^{b'}$ is the volume of the transformed phase divided by the volume of the solid phase only (the target composition) and X_s^α is the volume fraction of inclusion particles which is related to ρ in the same way. This relationship is valid only after the α-Al_2O_3 transformation, thus the calculated matrix densities of mixtures are compared in Fig. 11 with the density of unconstrained seeded boehmite heated above 1200 °C. It should be noted that the calculated matrix density is based on the total sample volume minus the space occupied by the coarse α-Al_2O_3 particles; the large voids shown in Fig. 6b are included in the matrix volume. The significantly lower ρ_m in the 70% mixture is partially due to these large voids, but for the 30% mixture, which does not have these type of voids, ρ_m is still lower than the unconstrained seeded boehmite. The large difference in the very early stage of sintering is due to the α-Al_2O_3 transformation and associated large specific volume change which is believed to influence further densification of the mixtures.

The matrix densification rate, $d\rho_m/dt$, is plotted in Fig. 12 for the mixtures and the unconstrained case. The matrix densification rates in the mixutres are significantly lower than the free matrix up to ~1300 °C. The temperatures for the maximum densification rate of the matrix in the mixtures are >100 °C higher than for the free matrix. Both the degree of decreased densification rate and the increase in the temperature for the maximum densification rate increase with increasing inclusion content. A similar analysis was carried out by Rahaman and De Jonghe [27] for ZnO containing 10 wt % SiC. They reported that the temperatures for the maximum densification rate are approximately the same for both the free and constrained matrix. In the present work, however, significant differences are observed between the temperatures for the maximum densification rate for the unconstrained and constrained cases. This result indicates

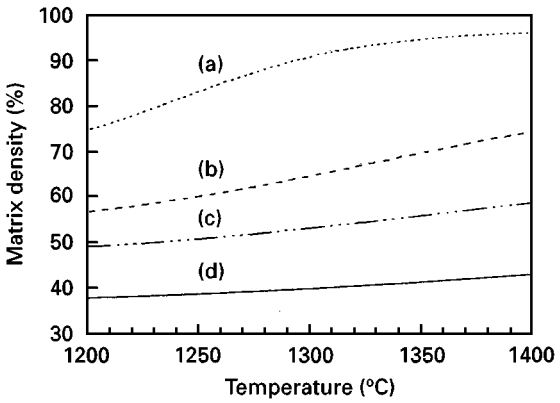

Figure 11 Matrix densities in (a) the seeded boehmite, (b) the 30% mixture, (c) the 50% mixture and (d) the 70% mixture.

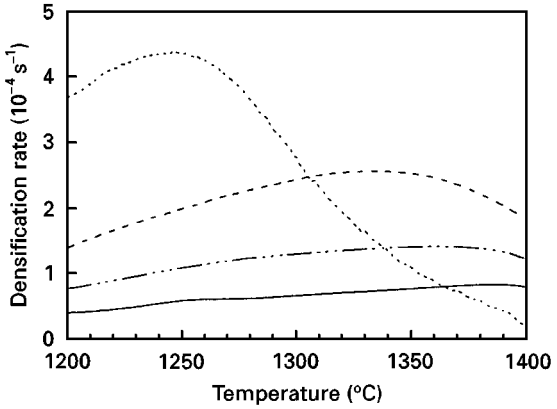

Figure 12 Matrix densification rate of: (···) seeded boehmite, (- - -) the 30% mixture (– ··· –) the 50% mixture and (——) the 70% mixture.

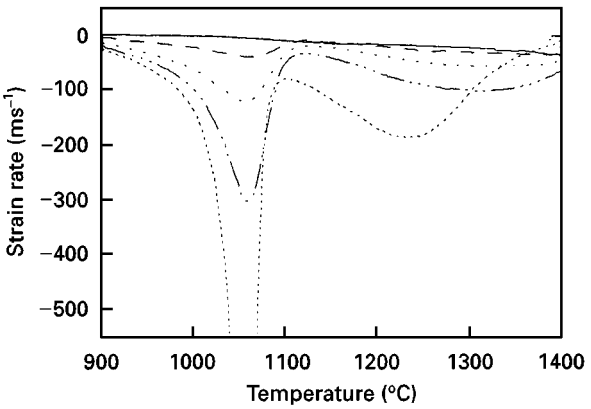

Figure 13 Strain rate of: (···) seeded boehmite, (– ··· –) the 30% mixture, (- - -) the 50% mixture, (– – –) the 70% mixture and (——) the 100% coarse.

a different mechanism for the retarded densification in boehmite/Al_2O_3 bimodal mixtures. Several possible reasons for this include a difference in inclusion fraction, interaction between inclusion and matrix (phase identity of matrix and inclusions [28]), and the mechanical response of the matrix.

In Fig. 13, the strain rates of the mixtures are plotted against temperature. Seeded boehmite shows two distinct peaks at 1050 and 1235 °C. The first large peak corresponds to the rapid volume change during the α-Al_2O_3 transformation. The second, relatively shallow peak results from densification of the transformed microstructure. The mixtures also have two peaks but the densification peaks shift to higher temperatures and intensities decrease as the course α-Al_2O_3 fraction increases. The peak intensity indicates how fast the sample densifies at a given temperature with a higher intensity meaning that the sample microstructure is more homogeneous and densification occurs in a narrower range of temperature. Densification peaks of the mixtures are shifted to higher temperatures by ~100 °C compared to the seeded boehmite and they are much shallower than the seeded boehmite. Amongst the mixtures, the temperature for the maximum densification rate increases slightly as the alumina fraction increases.

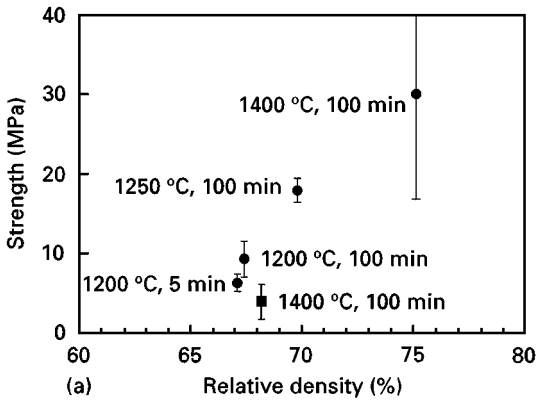

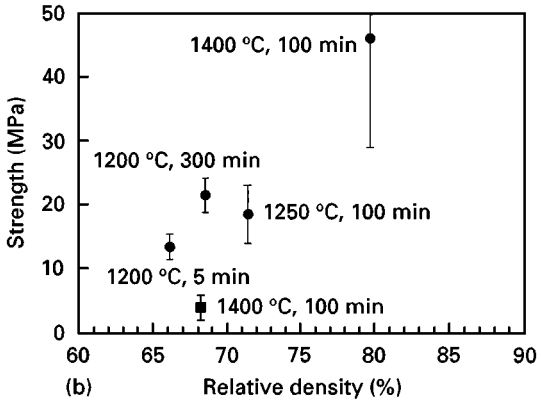

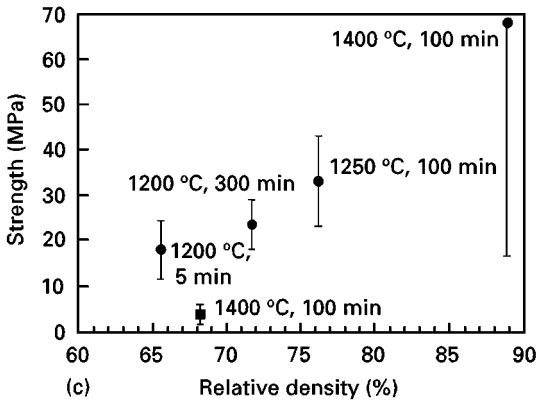

Figure 14 Diametral strength as a function of relative density of (a) the 70% mixtures, (b) the 50% mixtures and (c) the 30% mixtures. Note that on all three plots the value of the 100% mixture is represented by the (■) symbol.

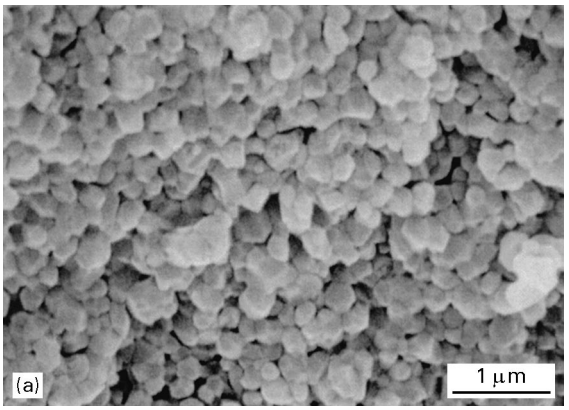

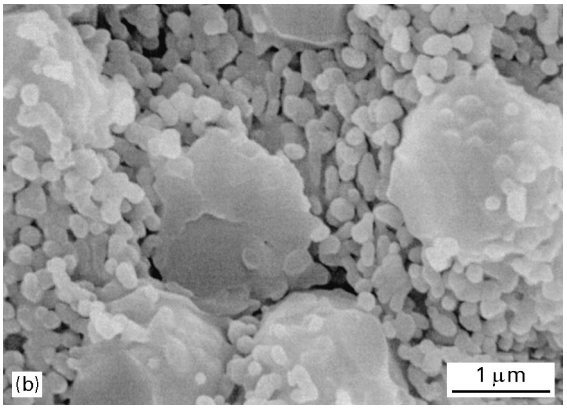

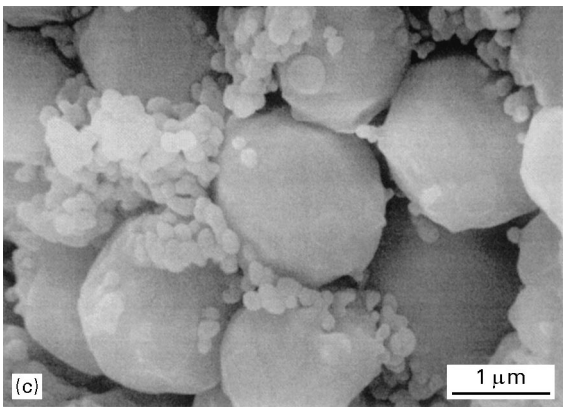

Figure 15 Fractured surface of samples sintered at 1200 °C for 300 min (a) seeded boehmite, (b) the 30% mixture and (c) the 70% mixture.

The increase of temperature of the maximum densification rate for the mixtures account for the constrained sintering, but the extent of the increase varies depending upon the parameters such as inclusion fraction and density of the matrix. In the densification rate of a ZnO matrix with 10 wt % SiC inclusion reported by Rahaman and De Jonghe [27], the temperature increase was not as pronounced as the present work. However, in the data reported by Sudre and Lange [15], a significant increase of the temperature for the maximum densification rate in the mixture with 30 % inclusion is observed. The difference in the temperature increase is basically due to the stress relaxation ability of the matrix or to the difference in the mechanisms for the constrained densification.

4.3. Strength

The strength of the mixtures is compared with the strength of the 100% coarse sample as a function of sintered density in Fig. 14 (a–c). The strength of the mixtures sintered at 1200 °C for 300 min is also compared with them. It is clear that for a given density, the mixtures have a higher strength compared to the 100% coarse sample. The increase in density for the prolonged time at 1200 °C is very small for the 70% mixture (0.5%) and it becomes larger with increased boehmite content.

For sintered type porous ceramics, the mechanical properties can be improved by sintering in the temperature range where surface diffusion is the predominant mechanism compared to that for volume diffusion; sintering at low temperature where the neck growth of a particle is predominant over the densification. The

strengths of the 70 and 50% mixtures are slightly above the line connecting the strength value of 1200 °C 5 min and 1250 °C 100 min. This implies that coarsening is more dominant when the inclusion fraction is high. In other words, the retardation for the 30% mixture is relatively smaller than other mixtures. The microstructures of samples sintered at 1200 °C for 300 min are shown in Fig. 15 (a–c). The difference in the shape of seeded boehmite and the fine particles in the mixture are more pronounced than after 5 min sintering. Seeded boehmite shows faceted crystallites whereas the fine particles in the mixtures rounded which implies that connectivity of the fine particles is an important factor for the densification.

The low density of the mixtures sintered at high temperatures (> 1400 °C) is due to network formation, but it is clear that densification is significantly constrained before the network forms. Microstructural observation reveals that, in the early stage of sintering (1200 and 1250 °C), the connectivity of the fine particles in the mixtures is poor compared to the unconstrained case. The poor connectivity is a result of the tensile stress in the matrix.

5. Conclusions

The retarded densification of a bimodal particle size powder can be utilized to fabricate porous alumina by mixing seeded boehmite and coarse α-Al_2O_3 particles. The phase transformation of boehmite and corresponding specific volume change along with inherent constraint resulted in a low transformed density and retarded densification. The poor mechanical strength of the coarse alumina particle compact can be improved by mixing with seeded boehmite and the pore size distribution can also be tailored by changing the composition of the mixtures. Microstructural observation reveals that the low sintered density of the mixtures can be mainly explained by the formation of a continuous network, but the poor connectivity of the fine particles at the early stage of sintering is also one of the reasons for the retarded densification of the mixtures. The shrinkage of the mixtures can not be predicted by a simple geometrical consideration because the shrinkage before the α-Al_2O_3 transformation is not accompanied by densification and consequently the constraint is less severe than in densification. In the present work, it is shown that the presence of the coarse particles resulted in porous ceramics in spite of other parameters such as green density, seeding of boehmite, and the sol stability [16] were not designed to produce porous ceramics. Consequently, changing these parameters can be another way of tailoring the pore size distribution.

Acknowledgement

The authors are grateful to Ssangyong Cement Industries Co., Ltd. in Korea for the financial support to Seongtae Kwon.

References

1. L. M. SHEPPARD, in "Ceramic transactions", Vol. 31, edited by K. Ishizaki, L. Sheppard, S. Okada, T. Hamasaki and B. Huybrechts (American Ceramic Society, Columbus, OH, 1993) p. 3.
2. C. J. BRINKER and G. W. SCHERER, in "Sol–gel science" (Academic Press, San Diego, 1990) p. 839.
3. J. S. WOYANSKY, C. E. SCOTT and W. P. MINNEAR, *Amer. Ceram. Soc. Bull.* **71** (1992) 1674.
4. K. UCHIDA, S. ISAMI, M. KIYOTSUKA and K. IWASAKI, in "Material science monographs," Vol. 66 D, edited by P. Vincenzini (Elsevier, Netherlands, 1991) p. 2639.
5. M. NANKO, K. ISHZAKI and A. TAKATA, in "Ceramic transations", Vol. 31, edited by K. Ishizaki, L. Sheppard, S. Okada, T. Hamasaki and B. Huybrechts (American Ceramic Society, Columbus, OH, 1993) p. 117.
6. M. WU and G. L. MESSING, *J. Amer. Ceram. Soc.* **73** (1990) 3497.
7. A. G. EVANS, *ibid.* **65** (1982) 497.
8. F. F. LANGE and M. METCALF, *ibid.* **66** (1983) 398.
9. R. RAJ and R. K. BORDIA, *Acta Metall.* **32** (1984) 1003.
10. R. K. BORDIA and R. RAJ, *Adv. Ceram. Mater.* **3** (1988) 122.
11. C. H. HSUEH, A. G. EVANS, R. M. CANNON and R. J. BROOK, *Acta Metall.* **34** (1986) 927.
12. R. K. BORDIA and G. W. SCHERER, *ibid.* **36** (1988) 2411.
13. G. W. SCHERER, *J. Amer. Ceram. Soc.* **70** (1987) 719.
14. F. F. LANGE, *J. Mater. Res.* **2** (1987) 59.
15. O. SUDRE and F. F. LANGE, *J. Amer. Ceram. Soc.* **75** (1992) 519.
16. S. KWON and G. L. MESSING, *J. Sol–Gel Sci. Technol.* **9** (1997) 53.
17. G. L. MESSING and G. Y. ONODA, JR., *J. Amer. Ceram. Soc.* **61** (1978) 1.
18. *Idem.*, *ibid.* **64** (1981) 468.
19. K. WEFERS and C. MISRA, in "Oxides and hydroxides of aluminum", Alcoa Technical Paper No. 19 (Aluminium Company of America, Pittsburgh, PA, 1987) p. 51.
20. R. B. BAGWELL and G. L. MESSING, in "Key engineering materials", Vol. 115, edited by D. M. Liu (Trans Tech Publications, Switzerland, 1995) p. 45.
21. R. S. ZHOU and R. L. SNYDER, *Acta. Cryst.* **B47** (1991) 617.
22. M. KUMAGAI and G. L. MESSING, *J. Amer. Ceram. Soc.* **68** (1985) 500.
23. J. L. MCARDLE and G. L. MESSING, *Adv. Ceram. Mater.* **3** (1988) 387.
24. *Idem.*, *J. Amer. Ceram. Soc.* **76** (1993) 214.
25. L. C. DE JONGHE, M. N. RAHAMAN and C. H. HSUEH, *Acta Metall.* **34** (1986) 1467.
26. M. J. O'HARA and I. B. CUTLER, *Proc. Brit. Ceram. Soc.* **12** (1969) 145.
27. M. N. RAHAMAN and L. C. DE JONGHE, *J. Amer. Ceram. Soc.* **74** (1991) 433.
28. D. Y. JENG and M. N. RAHAMAN, *J. Mater. Sci.* **28** (1993) 4421.

Received 27 January
and accepted 19 August 1997